Chapter 9

Semi-Alicyclic Polyimides: Insights into Optical Properties and Morphology Patterning Approaches for Advanced Technologies

Andreea Irina Barzic, Iuliana Stoica and Camelia Hulubei

Additional information is available at the end of the chapter

http://dx.doi.org/10.5772/53607

1. Introduction

Polyimides (PIs) represent a very important class of high performance synthetic polymers, characterized by stability at elevated temperatures, low thermal expansion, chemical resistance, low dielectric constant, high breakdown voltage, good optical transparency, high adhesion and dimensional stability [1-3]. Therefore, they have found widespread applicability: in microelectronics - as interlayer dielectrics, in aircraft industry - as thermo-resistant components and in optoelectronics - as optical waveguides. In recent years, some types of PIs were proven to be biocompatible [4], and they have been used in biomedical fields as flexible and implantable intracortical electrode arrays [5] and as microstructured substrates for contact guidance of cell growth [6], on condition of being patterned at micro or nanoscale. However, the strong intermolecular forces between the aromatic PI chains make them difficult to process because they decompose prior to melting and are insoluble in organic solvents [7-9]. One the other hand, the formation of intra- and intermolecular charge transfer complex (CTC) between the electron-donating diamine and the electron-accepting dianhydride moieties explains the coloration ranging from pale yellow to deep brown, causing strong absorption in the visible region [10,11], and enhance the dielectric constant. All these problems greatly limit the widespread use of aromatic PIs in areas where colorlessness and transparency are required, for example, as covers for solar cells, orientation films in liquid crystal display (LCD) devices, optical waveguides for communication interconnectors and other high-tech fields. An intensive research effort has been undertaken to counteract these shortcomings by designing their structure, including: (1) increasing flexibility along the polymer chain by employment of flexible (*e.g.* –O–,–SO_2–, –CH_2–, NHCO–) or less symmetric links, such as meta- or ortho-catenated aromatic units, (2) introducing bulky pendant groups and biphenyl units onto the backbone, and (3) utilizing

fluorinated monomers [12]. One of the most successful approaches to enhance transparency, to decrease the dielectric constant and simultaneously to improve solubility consisted in incorporation of aliphatic monomers in the PI backbone, which lead to development of a new type of PIs, namely aliphatic ones [13-17], but in this case the thermal stability is compromised [14]. Partially aliphatic PIs are occupying an intermediate position between aromatic and aliphatic derivatives; they combine the advantages of both. Cycloaliphatic monomers impart the thermal properties similar to that of aromatic ones since they foster less probability of main chain scission because of the presence of multibonds, while they offer improvements in transparency and dielectric constant since they are free of CTC [13]. Moreover, it is well known that utilization of biologically inert and nontoxic monomers leads to a greater mechanical stability during exploitation, allowing the polymer existence in a living organism without negative consequences. Comparatively to other aliphatic tetracarboxylic dianhydrides used as raw materials for PIs, Epiclon (5-(2,5-dioxotetrahydrofuryl)-3-methyl-3-cyclohexene-1,2-dicarboxylic acid anhydride) is a unique bulky, flexible and asymmetrical chemical structure, rendering new properties to the resulting compounds [18-25]. Refractive index, optical transparency, energies describing the absorption edge and surface morphology patterning approaches of some polyimides based on Epiclon and aromatic diamines containing flexible sequences are presented in this chapter, in correlation with their potential applications.

2. Synthesis approach and thermal stability of some new semi-alyciclic PIs based on Epiclon

The adopted strategy used to obtain novel semi-alicyclic PIs is focused on obtaining a proper balance between thermal and physical properties and solubility. The synthesis approach involves the control of chain flexibility and segmental mobility through the incorporation of cycloaliphatic groups and flexible linkages, so that to weaken the strong intra- and intermolecular interactions by disrupting coplanarity and conjugation, reducing symmetry, and separating electronic segments [26]. In this context, in order to obtain soluble PIs, with enhanced transparency and insulation properties, the backbone was chemically modified/designed by:

- incorporation of alicyclic dianhydride: Epiclon (98% purity, Merk) to increase the solubility (due to the less polymer–polymer interactions) and thermal stability (due to the multibond and rigidity of the alicyclic structure) [27];
- incorporation of flexible linkages (–O–, $–CH_2–$, $– (CH_2)_2–$) to introduce "kinks" to the polymer chain which decrease the rigidity, inhibit the packing, reduce the intermolecular interactions, weaken the intensity of the yellow color, and increase the solubility [28].

The new polyimides **PI1-PI5** were synthesized by solution polycondensation of equimolar amounts of Epiclon with five diamines containing different flexible sequences, namely: *p*-phenylenediamine (PPD), 4,4'-methylenedianiline (DDM), 4,4'-ethylenedianiline (DDE), 4,4'-oxydianiline (ODA) and 1,4-bis(*p*-aminophenoxy)benzene (PDA). The reactions were carried

out in N-methylpyrrolidinone (NMP), as solvent, under inert atmosphere (Scheme 1) [22-25]. Concentration of the reaction mixture was adjusted to 20% total solids. The first step of this reaction performed under completely anhydrous conditions at 15-20°C, led to the poly(amic acid)s (**PAA1-PAA5**). In the second step, the polymer solution was heated to 180-190°C to perform the cyclodehydration of the poly(amic acid) to the corresponding polyimide structure (**PI1-PI5**).

Polyimide films were prepared through imidization of PAA films cast on a glass substrate, which were placed overnight in an 80 °C oven to remove most of the solvent. The semidried PAA films were further dried in an oven and transformed into PIs, by the following heating program: 120 °C, 160 °C, 180 °C, 210 °C and 250 °C for 1h at each temperature. After stripping the films in hot water, the resulting samples were dried at 65 °C in a vacuum oven for 24 h. The thermal imidization leads to cross-linked, partially aliphatic PI films, since the special structure of the Epiclon dianhydride (Scheme 1) [22-25,29] is different from that of conventional PIs.

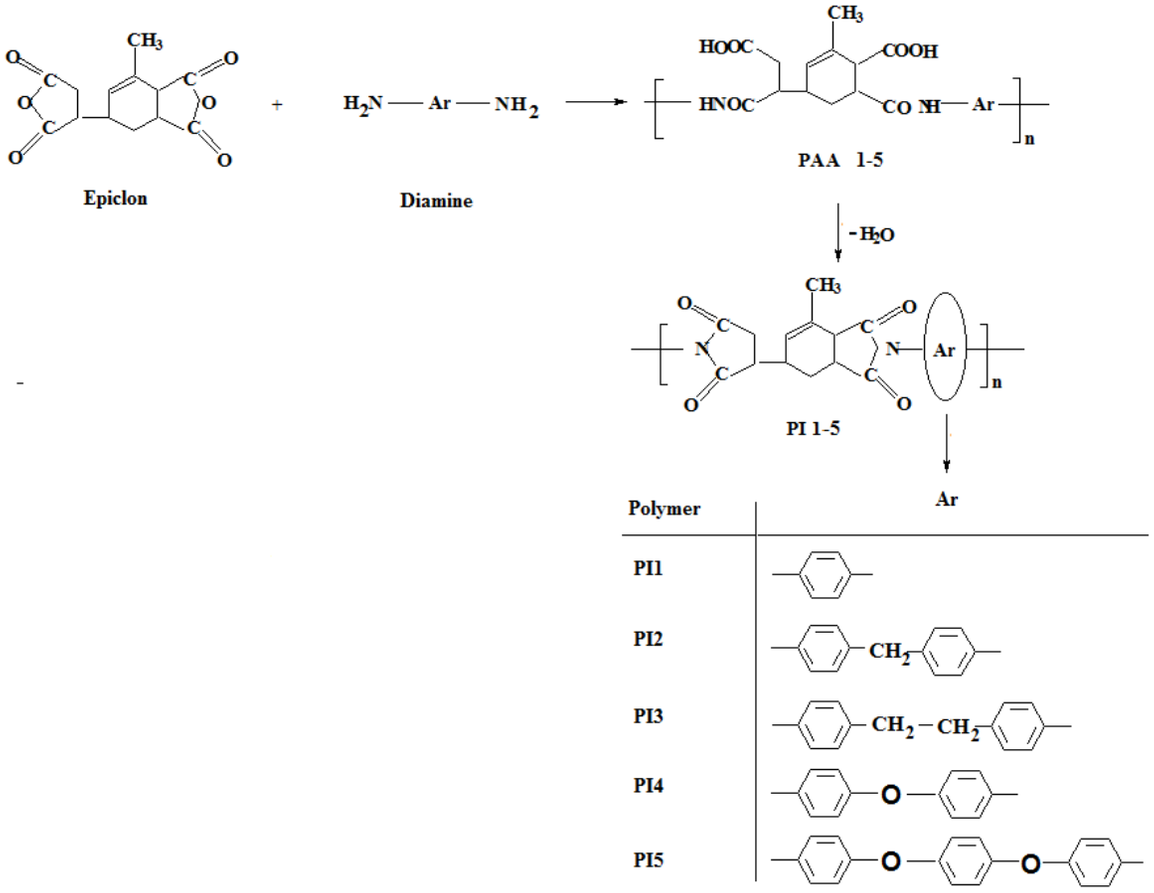

Scheme 1. Synthesis of the Epiclon-based polyimides

The number average molar mass, M_n, and the polydispersity index, M_w/M_n, for the PIs (Table 1) were determined by gel permeation chromatography (GPC) measurements in N,N-dimethylformamide (DMF), on a PL EMD-950 evaporative light scattering detector apparatus. Considering that the polymerization degrees of the PAAs and of the

corresponding PIs are identical, the number-average molar mass, M_n, of the PAAs was determined from the polymerization degree of the polyimides (M_n/m_{PI}) and the molar mass of the structural units of poly(amic acid)s, m_{PAA}, according to Table 1 [30].

Conversion of PAAs to fully cyclized PIs was determined by FTIR vibrational spectroscopy. The absorption bands most frequently used for determining imide formation are 1780 cm^{-1} (C=O asymmetrical stretching), 1720 cm^{-1} (C=O symmetrical stretching), 1380 cm^{-1} (C-N stretching), and 725 cm^{-1} (C=O bending) [31,32]. The amide bands at 1660 cm^{-1} (C=O) and 1550 cm^{-1} (CONH), which may also appear as broad peaks, are useful for qualitative assessment of the imidization degree [33,34]. The polymers containing Epiclon moieties showed characteristic peaks at 2930–2920 cm^{-1}, associated with the aliphatic sequences. In Figure 1 is exemplified the FTIR spectra of the PI1 and PI4. It can be observed that the broad absorption band at 3350–3450 cm^{-1}, characteristic to amidic NH, and the narrow absorption peak at 1650–1660 cm^{-1}, due to the C=O groups in amide linkage, entirely disappeared, indicating completion of thermal imidization of the intermediate polyamidic acid into a final PI structure, confirming the successful synthesis of polymers.

Sample	m_{PAA}	M_n , g/mol	Sample	m_{PI}	M_n , g/mol	M_w/M_n	IDT,°C	$T_{g,\,PI}$,°C
PAA1	372	63 000	PI1	336	57 000	1.28	270	258
PAA2	462	53 000	PI2	426	50 000	1.59	273	255
PAA3	476	75 000	PI3	440	70 000	1.27	274	246
PAA4	462	76 000	PI4	426	48 000	1.31	281	235
PAA5	556	77 000	PI5	520	75 000	3.36	280	230

Table 1. Molar mass of chain units, m, number average molar mass, M_n and polydispersity indices, M_w/M_n, of poly(amic acid)s and polyimides [21,23,25,29,30]

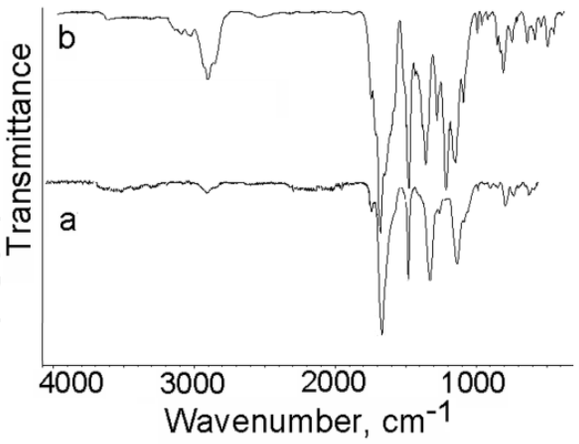

Figure 1. FTIR spectra for (a) **PI1** and (b) **PI4** samples

The thermal stability of the Epiclon-based PIs (Table 1) was evaluated by thermogravimetric analysis (TGA) and differential scanning calorimetry (DSC). The PIs exhibit an initial decomposition temperature (IDT) in the range of 270-281°C. The glass transition temperature (T_g) of PIs was probed the by monitoring the heat capacity as a function of temperature. The T_g could be considered as the temperature at which a polymer undergoes

extensive cooperative segmental motion along the backbone. Table 1 presents the T_g's of resulting PIs that differ in diamine structure. In particular, the chain stiffness has been found to have an important influence on the T_g values. The presence of flexible linkage increased the polymer chain flexibility by decreasing the energy of internal rotation [35], thereby lowering the T_g as is evident from Table 1, showing that the flexible diamines containing ether-linkages exhibit a little lower T_g values. The cycloaliphatic structure of Epiclon renders to the resulting PIs good thermal resistance and also improves other properties, especially the optical ones [36].

3. Refractive index, optical gap and absorption edges

Since in applying PIs to optical and electrical use the refractive index is one of great importance, this parameter must be evaluated in correlation with the chemical structure. Ellipsometry is a modern technique that uses polarized light to probe the refractive index, absorption coefficient and optical gap. The method allows evaluation of these parameters from the correlation between the incidence angle, the amplitude of reflected and incident electric field ratio, and their phase difference, which are related to the ratio of Fresnel reflection coefficients. Variable angle ellipsometry performs measurements as a function of wavelength and angle of incidence. Because ellipsometers measure ratios of two values they are accurate and reproducible, even at low light levels, and no reference material is necessary. The dependence of the ellipsometric parameters on the incidence angle is important in electing the correct mathematical model for determination of the optical constants. The basic ellipsometry equation is [37]:

$$\tan\Psi e^{i\Delta} = \rho = \frac{r_p}{r_s} \tag{1}$$

where r_p and r_s are the complex Fresnel reflection coefficients for p and s polarized light (polarized in the incidence plane or perpendicular to it, respectively).

The refractive index, n, and extinction coefficient, k, values were calculated from the measured values of ellipsometric angles Ψ and Δ, using equation (2):

$$(n+jk)^2 = \sin^2\theta\left\{1+\tan^2\theta\left[\frac{1-\tan\Psi e^{j\Delta}}{1+\tan\Psi e^{j\Delta}}\right]^2\right\} \tag{2}$$

where θ is the incidence angle.

Figure 2 presents the dependence of the ellipsometric parameters Ψ and Δ on the incidence angle for the Epiclon-derived PIs. The shape of this dependence is important in electing the correct mathematical model for determination of the optical constants. Using the principal angle ellipsometry method ($\Delta = -\pi/2$) [37], the equation (2) becomes as shown in relation (3):

$$(n+jk)^2 = \sin^2\theta_p\left[1+\tan^2\theta_p\left(\cos 4\Psi_p + j\sin 4\Psi_p\right)\right] \quad (3)$$

where: θ_p is the principal incidence angle.

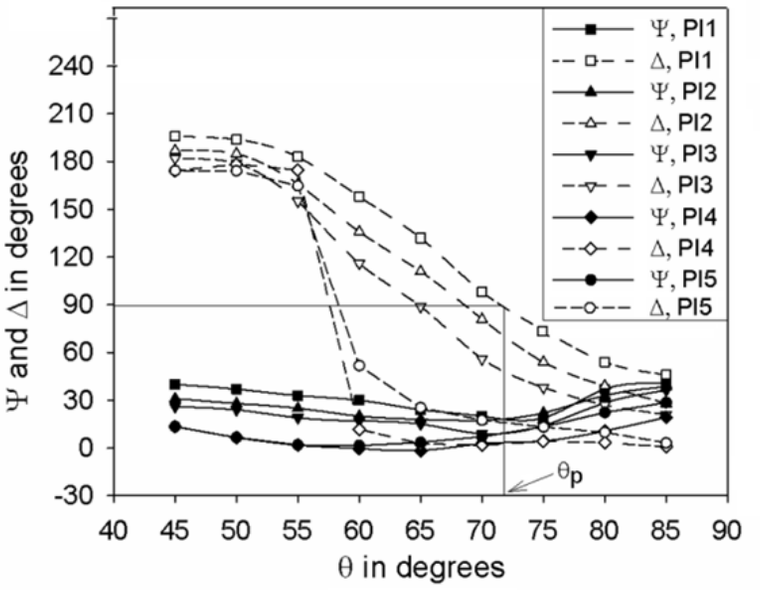

Figure 2. Dependence of the ellipsometric parameters Ψ and Δ on the incidence angle for Epiclon-derived PIs

The low polarizability provided by the alicyclic Epiclon moieties leads to PIs with low refractive index. The ellipsometricaly measured values listed in Table 2 show that refractive indices of this type of PIs measured at 632.8 nm correspond to transparent materials, *i.e.* 1.6-1.7, and are in good agreement with theoretical estimations based on molar refraction and molar volume derived from group contributions theory [29,36]. This approach is based on the assumption that the molar volume, V_u, and the molar refraction, R_u, of the chain repeating unit are additive functions of composition:

$$V_u = \sum_i a_i \cdot V_i \quad (4)$$

$$R_u = \sum_i a_i \cdot R_i \quad (5)$$

where V_i and R_i are the contributions of group, and a_i is the number of groups i in the repeating unit.

The increments of various substructures R_i and V_i were taken from the literature [38,39]. The refractive index of Epiclon based polyimides were determined by equation proposed by Lorenz-Lorentz [40,41]:

$$R_{u,LL} = V_u\left(n_{LL}^2 - 1\right)/\left(n_{LL}^2 + 2\right) \quad (6)$$

The experimental values of the refractive index for these semi-alicyclic PIs slightly differ from those calculated with the Lorenz-Lorentz equation, on considering the corresponding group contributions to the molar refraction and to the molar volume.

Both refractive index and extinction coefficient, *k*, are influenced by the aromatic character of the diamines used in synthesis. The decrease of the charge transfer interactions is reflected by a small probability of optical transitions and implicitly by low values of n and k.

Samples	R_i (cm^3/mol)	V_i (cm^3/g)	n_{LL}	$n_{ellipsom}$	k	$\varepsilon' = (n_{ellipsom})^2$
PI1	82.076	209.163	1.713	1.725	2.883	3.273
PI2	111.815	290.603	1.691	1.683	2.209	3.115
PI3	116.319	306.131	1.685	1.646	1.808	2.980
PI4	108.936	284.127	1.693	1.615	0.097	2.869
PI5	135.796	359.091	1.681	1.611	0.092	2.855

Table 2. Theoretical and experimental refractive index, extinction coeficient and dielectric constant values of Epiclon-derived PIs

The control of refractive index, n, of polyimides also means the control of dielectric constant (ε') according to Maxwell's relation $\varepsilon' = n^2$. Therefore, ε' around 1 MHz is evaluated to be equal about 1.1 times n square including an additional contribution of approximatively 10% from the infrared absorption, that is $\varepsilon' = 1.1n^2$. Materials with relatively low dielectric constants provide effective electrical barrier properties. A lower dielectric constant indicates that the respective material is suited for protection and insulation in microelectronics. In multilevel electronics packaging, an important function of a dielectric material is to block the electromagnetic interactions between parallel metal conducting lines, which operate independently. For assuming an effective blocking the material should have low ε'. The dielectric constant is used to describe a material's ability to store the charge, when used as a capacitor device. Materials with dielectric constants below 4.0, which correspond to the value of the standard SiO_2 insulator, have been recognized by the electronics industry as being superior in electrical performance to ceramics. For this reason, when polyimide films are used as interlayer dielectrics in microelectronic packaging, the pulse propagation delay is proportional to ε' of the polymer and accordingly, the reduction of ε' allows faster machine time concurrently with lower crosstalk noise.

Generally, the literature shows that for polyimides the dielectric constant decreases gradually with increasing frequency. This variation is attributed to the frequency dependence of the polarization mechanisms which include the dielectric constant. The magnitude of the dielectric constant is dependent on the ability of the polarizable units in a polymer to orient fast enough to keep up with the oscillations of an alternating electric field. At optical frequencies (approx. 10^{14} Hz), only the lowest mass species, the electrons, are efficiently polarized. At lower frequencies, the atomic polarization of nuclei, which move more slowly, also, contribute to the dielectric constant. Atomic polarization of induced

dipoles such as a carbonyl group may occur in infrared (10^{12} Hz) or lower frequency regimes. Dipole polarization represents the redistribution of charge when a group of atoms with a permanent dipole align in response to the electric field. In solid state, the alignment of permanent dipoles requires considerably more time than electronic or atomic polarization, occurring at microwave (10^9 Hz) or lower frequencies. The contribution of each polarization mode to the dielectric constant is expressed in equation (7):

$$\varepsilon = \varepsilon_{electronic} + \varepsilon_{atomic} + \varepsilon_{dipolar} \quad (7)$$

At optical frequencies, when only electronic polarization occurs, the dielectric constant is related to the refractive index by Maxwell's identity. A comparison between ε' values at different frequencies may assure a basic understanding of the influence of the molecular structure on the dielectric properties of Epiclon-based PIs.

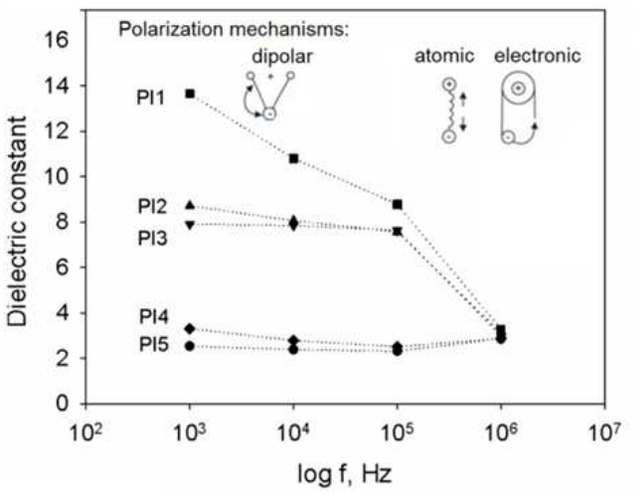

Figure 3. Dielectric constant dependence on frequency for Epiclon-derived PIs. The ε' values at 1 kHz, 10 kHz and 100 kHz were experimentally obtained on a LCR METER, while those at 1 MHz were estimated by Maxwell's identity using ellipsometrical measurements

Introduction of different Ar structures in PI backbone determines variation of the free volume by changing of the polarizable group number per unit volume, which leads to the modification of polymer densities and, implicitly, of the dielectric constants. Thus, according to literature data [42,43], a higher free volume determines a lower dielectric constant. In Figure 3 it can be observed that dielectric constants of Epiclon-derived PIs containing ether bridges are around 2.8 at 1 MHz, recommending this type of PIs as interlevel dielectric layers in the fabrication of semiconductor chips and multichip packaging structures [44].

On the other hand, PIs containing cycloaliphatic structures are expected to have better transparency than aromatic ones, due to the prohibition of electron conjugation by the introduction of alicyclic moieties [45]. This property is a key factor in visualization of the cell culture morphology development on the patterned polymer substrate, but it is also required to obtain liquid crystal devices with good quality. Optical transparency of Epiclon-derived PI films was evaluated in the range of 290-1100 nm (Figure 4). The combination in the PI

backbone of cycloaliphatic Epiclon moieties with aromatic diamine residues containing different flexible sequences leads to a transmittance of appreciatively 90% over visible domain. The transparency band can be extended to UV region depending on the diamine chemical structure. The cutoff wavelength (at which transmittance is 1%) is lower as the diamine chain length is shorter, namely 316 nm – value comparable to that of a fully alicyclic PI [14].

To obtain the energy gap and other energies describing the absorption edge, the method proposed by Tauc for amorphous semiconducting materials is applied. Then, on the basis of these values, the influence of polymer chain structure and structural disorder on the optical properties and probable electronic transitions can be considered. In order to determine the absorption coefficient a from the transmission data, the expression (8) was used:

$$\alpha = (1/d)\ln(1/T) \tag{8}$$

where d is the film thickness (approx. 40 μm) and T is the transmittance.

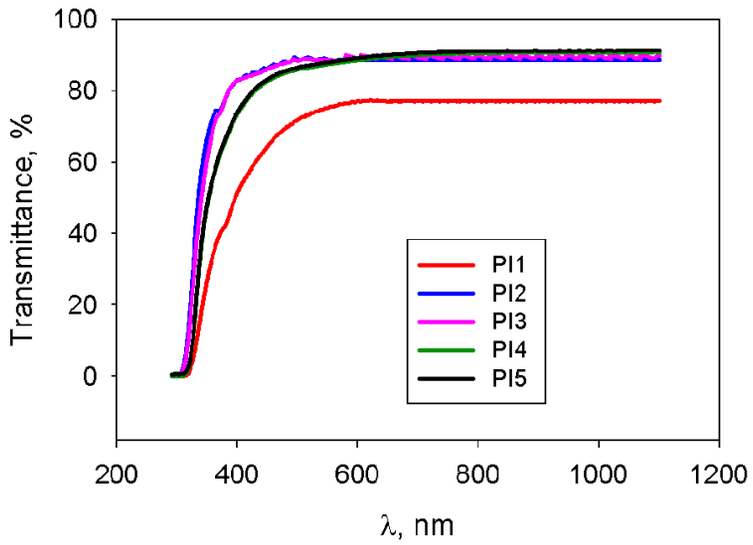

Figure 4. Typical overall transmission spectra of Epiclon-based polyimide films

Generally, for a typical amorphous semiconductor, three domains are evident in the variation of the absorption coefficient *versus* photon energy:

- in the first region, the absorption coefficient due to interband transition near the band-gap describes the optical gap energy E_G in amorphous semiconductors;
- in the second region, absorption at photon energy below the optical gap depends exponentially on photon energy, which defines the Urbach edge energy, E_U. The theories of the Urbach edge are based on the idea that the sharp absorption edge is broadened by some kind of mechanisms. For example, in semiconductors, the exponential edges are due to the electric fields produced by charged impurities. Besides the charged impurities, there are also other possible sources of internal electric fields. One of them is represented by density fluctuations via the piezoelectric effect in

semiconductors, with a piezoelectric constant different from zero. In amorphous materials, these density fluctuations do not change with time, so that the exponential edge can be thought of as due to frozen-in longitudinal optical phonons;

- the third region describes the optical absorption generated by defects appearing at an energy lower than the optical gap energy. This energy, E_T, the so-called Urbach tail, refers to the weak absorption tail and describes the defect states; this energy is rather sensitive to the structural properties of the materials. The absorption tail lies below the exponential part of the absorption edge (the second region), and its strength and shape were found to depend on the preparation, purity and thermal history of the material, varying only slightly with its thickness.

From the transparency data, the absorption coefficient was plotted in Figure 5 for Epiclon-based polyimide films, as a function of photon energy, according to equation (9):

$$\alpha = \alpha_0 \exp(E / A) \tag{9}$$

where α_0 is a constant and E is the photon energy.

The shape of all curves is very similar to the behavior proposed by Tauc for a typical amorphous semiconductor [46-48], the level of absorption (10^1–10^3 cm^{-1}) is lower than for amorphous, inorganic thin films. These results agree with other literature data [49,50], which assume that a lower absorption in polymer materials is due to a lower degree of bonding delocalization. An absorption edge is a sharp discontinuity in the absorption spectrum by an element appearing when the photon energy corresponds to the energy of a shell of the atom. Each of the absorption edges in Figure 5 exhibits two different slopes, and a saturation region for higher energies. Parameter A becomes either E_U, in the high-energy region, or E_T, in the low-energy region of absorption, according to the slopes exemplified in Figure 5 for Epiclon-derived PIs.

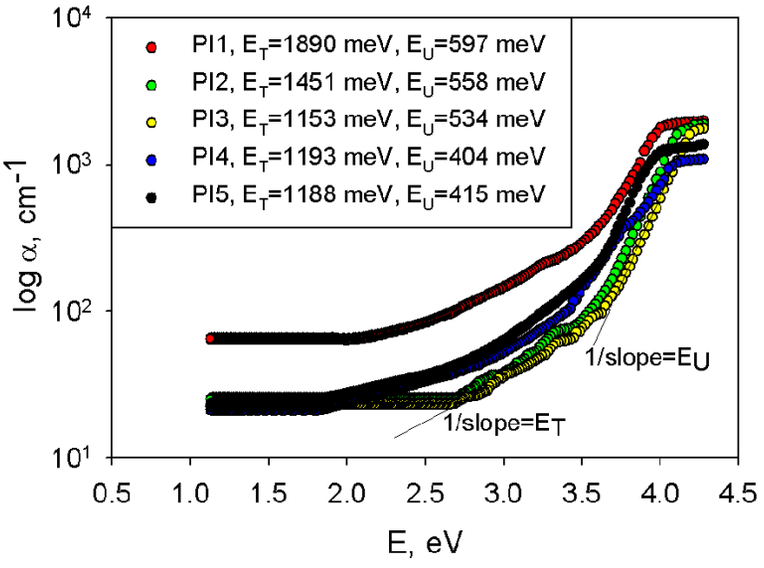

Figure 5. Absorption coefficient dependence on photon energy for Epiclon-based polyimide films

In the case of the Epiclon-based polyimide films, the absorption edges were found to follow the Tauc power law expressed in equation (10), in the range over which photon energy was higher than optical gap energy, E_G:

$$\left(\alpha \cdot E\right)^{1/2} = B\left(E - E_G\right) \tag{10}$$

where B is a constant.

The dependencies plotted in Figure 6 were used to obtain the Tauc optical gap energy, E_G. This approach, typical for amorphous semiconductors, has been also applied by us earlier for amorphous polymer films [51]. The values of optical gap energy higher than 3.26 eV are a good indicative of transparent polyimide films [50]. Also, Urbach and Tauc energies are distinctly lower as the conjugation in the aromatic structure and/or the intermolecular and intramolecular charge-transfer interactions are diminished [52]. These two optical energies are describing the absorption edges in rapport with the localized states induced by the polymer atomic structure. Such possible structure defects like the break, the abbreviation or the torsion of polymer chains, seem to be responsible for low-energy absorption, described by the Tauc parameter. Therefore, optical properties can be correlated with surface morphological aspects, offering useful insights for obtaining polyimide films for advanced microelectronic applications and bio-technologies.

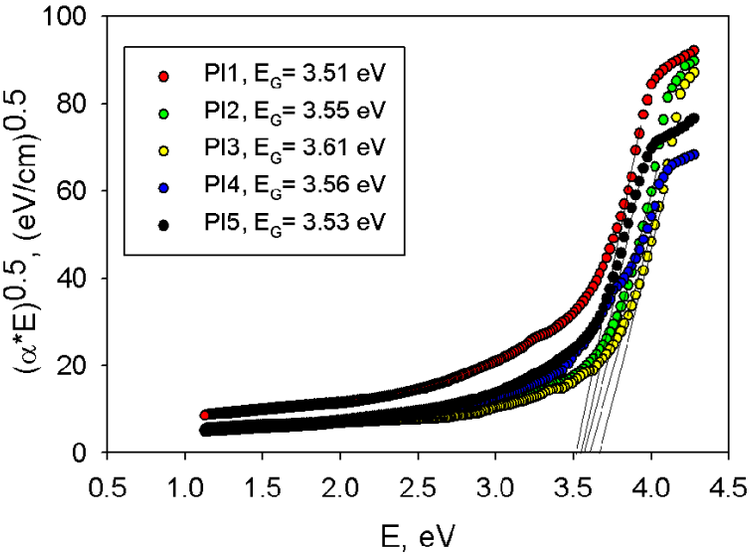

Figure 6. The Tauc dependence of Epiclon-based polyimide films

4. New insights on polyimide surface morphology and on patterning approaches

The characterization of PIs morphology involves a variety of different microscopic techniques such as optical microscopy (OM), scanning electron microscopy (SEM) and atomic force microscopy (AFM). Among them, AFM has proved to be a useful and attractive

tool to examine the surface topography and the possible existing defects. Moreover, AFM in tapping mode is suitable for soft PI films and can provide high resolution surface topographical and surface distribution data on the nanoscale. Besides the preparation history, the chemical structure determines the developed PIs morphology, which can be more carefully examined through the surface texture parameters. They can be accurately evaluated only using this method. In analyzing PI surface characteristics there are no studies (to our knowledge), which take into consideration these parameters.

The morphological features of PIs play an important role in various applications, such as tissue engineering - where the cell morphology can be controlled through polymer topography - or in liquid crystal displays (LCDs) - where the tilt angle of the liquid crystal (LC) molecules can be optimized by PI substrate. However, for these purposes the PI surface must be properly adapted [53]. In this sub-chapter are presented several surface processing techniques particularized for the above discussed semi-alicyclic PIs. Discussion of the results will try to highlight new aspects in explaining the surface ordering mechanisms and in patterning approaches.

4.1. Surface texture parameters

Three-dimensional surface topography techniques and parameters can be successfully applied in characterizing polyimide surfaces, even after they have been subjected to certain surface modification processes. Recently, specific 3D parameters, also called S-parameters, have been implemented. They are calculated from three-dimensional topographic data measurements [54]. In the last ten years efforts to standardize these 3D parameters have been made. Therefore, the European consortium divided roughness parameters into four general categories: amplitude parameters (based on overall height), spatial parameters (based on frequencies of occurrence of characteristics), hybrid parameters (based on the combination of height of the formations and frequencies of occurrence) and functional parameters (based on suitability for certain applications). Some of them are presented in Table 3 and they are used to emphasize the character of the surface formations, the wear ability of the surface, the fluid retention and the orientation of structuring.

Therefore, atomic force microscopy (AFM) was used to examine the Epiclon-based polyimide films and to measure their surface topography. Figure 7 plots the 3x3 μm^2 bidimensional representation of the surface morphology (small image from the right corner), material ratio curves and height histograms obtained for polyimides **PI1-PI5** and used for surface texture parameters determinations. As it can be observed, all the samples showed uniform and smooth surface morphology, derived mainly from the characteristics of the polymer chains that govern aggregation and molecular ordering, which occur during drying and thermal imidization processes. Bearing curve illustrating the three areas of interest used for calculation of the functional parameters: Sbi, Sci and Svi is presented in Figure 8.

Roughness parameters	Description	Symbol	Unit
Amplitude parameters	Average height	Ha	nm
	Average roughness	Sa	nm
	Root mean square roughness	Sq	nm
	Peak Height	Sp	nm
	Valley Depth	Sv	nm
	Peak to Valley Height	St	nm
Spatial parameters	Texture Direction of a surface	Std	deg
	Texture Direction Index	Stdi	
	Texture Aspect Ratio of a surface	Str	
Hybrid parameters	Surfaces Area Ratio	Sdr	%
	Projected Area	S2A	nm^2
	Surface Area	S3A	nm^2
Functional parameters	Surface Bearing Index	Sbi	
	Core Fluid Retention Index	Sci	
	Valley Fluid Retention Index	Svi	
	Peak Material Volume	Vmp	ml/m^2
	Core Material Volume	Vmc	ml/m^2
	Core Void Volume	Vvc	ml/m^2
	Valley Void Volume	Vvv	ml/m^2

Table 3. Tridimensional surface roughness parameters listed by their name, symbol and unit

Height distribution analysis was used to estimate the peak height (defined as the largest peak height value from the mean plane within the sampling area), the valley depth (defined as the largest valley depth value from the mean plane within the sampling area) and the peak to valley height (defined as the sum of the largest peak height value and the largest valley depth from the mean plane within the sampling area). The higher values of these parameters obtained for **PI1** and **PI5** films (Figure 7) were reflected also by a higher rms roughness (the root mean square of the surface departures from the mean plane within the sampling area) of the 2.35 nm and 1.60 nm and average roughness (the arithmetic mean of the absolute distances of the surface points from the mean plane) of 1.82 nm and 1.27 nm (Table 4). For the other PIs the roughness values were below 1 nm. Material ratio curve, also known as Abbot-Firestone curve (Figure 7, gray plot), is the integral of the amplitude distribution function (ADF/Surface Histogram). It is a cumulative probability distribution and a measure of the material to air ratio expressed as a percentage at a particular depth below the highest peak in the surface. At the highest peak, the material to air ratio is 0%, where the material to air ratio at the deepest valley is 100%.

The functional parameters [55], such as surface bearing index (the ratio of the RMS deviation over the surface height at 5% bearing area) core fluid retention index (the ratio of the void volume of the sampling area at the core zone divided by the RMS deviation) and valley fluid retention index (the ratio of the void volume of the sampling area of the valley zone divided by the RMS deviation) are computed directly from this curve. The evaluation of Sbi, Sci and

Svi indicates that the bulky and asymmetric molecule of Epiclon induces a good fluid retention in the core and valley zone and good bearing properties of the corresponding polyimides – aspect useful in membrane industry and in cell culture substrates.

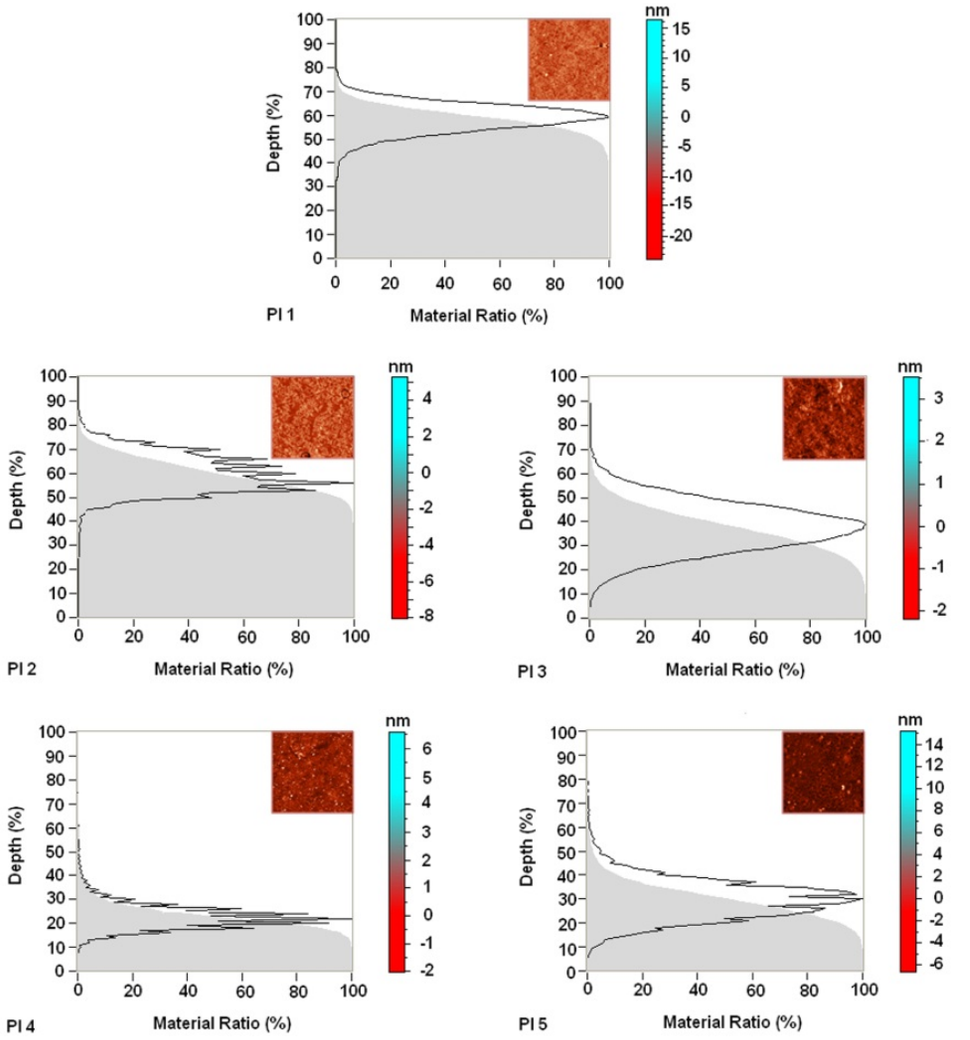

Figure 7. Amplitude distribution curves and height histograms used for surface texture parameters determinations for Epiclon-derived PIs. Each insert shows corresponding 3x3 μm² bidimensional topographical image

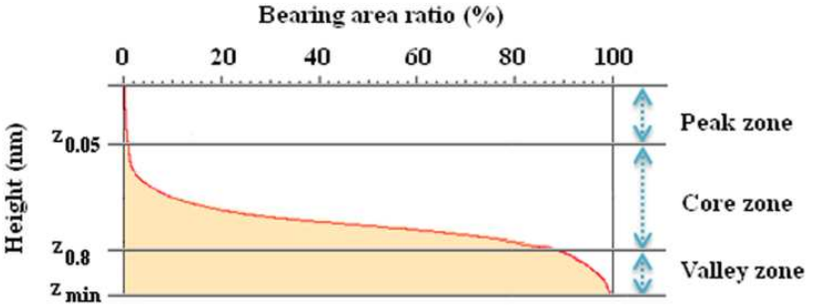

Figure 8. Bearing curve illustrating the three areas of interest used for calculation of the functional parameters: Sbi, Sci and Svi

Surface texture parameters	Samples				
	PI 1	PI 2	PI 3	PI 4	PI 5
Sa (nm)	1.82	0.81	0.42	0.33	1.27
Sq (nm)	2.35	0.97	0.53	0.48	1.60
Sp (nm)	15.31	4.77	3.15	5.28	8.75
Sv (nm)	10.95	4.37	1.77	1.95	5.01
St (nm)	26.25	9.14	4.92	7.23	13.76
Stdi	0.83	0.82	0.70	0.75	0.72
Str	0.70	0.64	0.38	0.54	0.65
Sbi	0.20	0.31	0.24	0.11	0.26
Sci	1.38	1.64	1.58	1.53	1.54
Svi	0.13	0.07	0.12	0.08	0.11

Table 4. Surface texture parameters for polyimides **PI1-PI5** calculated form height histograms, amplitude distribution curves and angular spectra

Tridimensional AFM images and corresponding angular spectra depicted in Figure 9 were used to estimate the spatial properties, related to the frequencies of occurrence of some features.

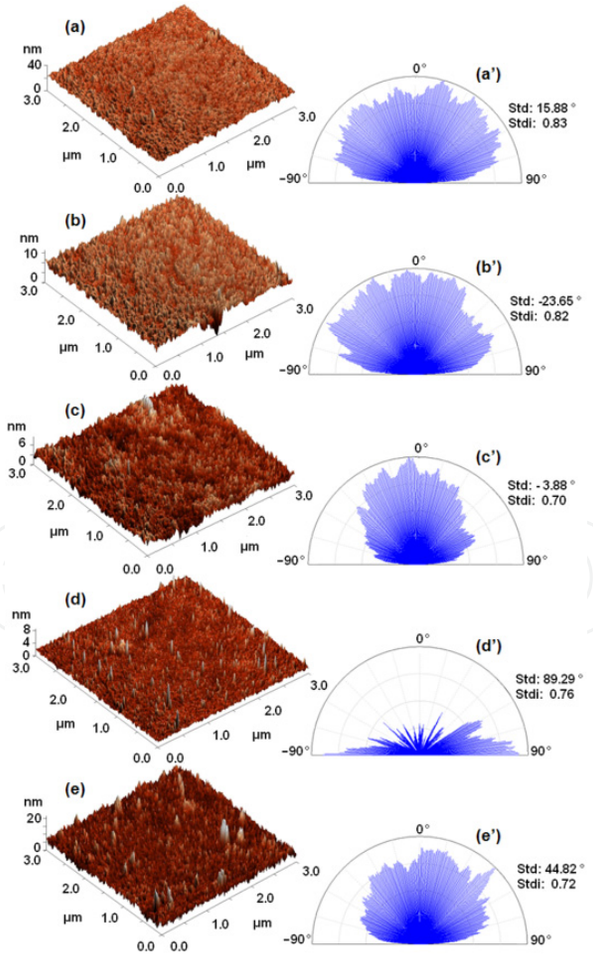

Figure 9. Tridimensional AFM images and corresponding angular spectra obtained for **PI1** (a, a'), **PI2** (b, b'), **PI3** (c, c'), **PI4** (d, d') and **PI5** (e, e') polyimide films

These can be described by parameters such as texture direction [55] (defined as the angle of the dominating texture in the image), texture direction index [56] (defined as the average amplitude sum divided by the amplitude sum of the dominating direction) and texture aspect ratio (used to identify the uniformity of the texture of the surface). For all the films, the texture direction index values (Stdi) were close to 1 (Table 4), indicating that the surfaces do not have a predominant texture direction (there is no significant lay to the surface) and the amplitude sum of all direction is almost similar. Moreover, the Epiclon-based PIs have the Str parameter higher than 0.3, revealing the isotropic character of the morphology (the surface has the same characteristics in every direction). AFM studies reveal that the enhancement of roughness is generated by the structural peculiarity of these polyimides which contain bulky, alicyclic dianhydride moieties and aromatic diamine residues with different flexibility [57]. The functional and spatial properties obtained for the discussed PI films indicate that these materials present good adhesion with circuit inorganic components, being suited as interlevel dielectric layers.

4.2. Novel aspects in patterning polyimide surface morphology

Depending on the nature of their precursors – the poly(amic acid)s – the polyimide microstructures can be typically patterned, either by direct photolithography of photosensitive type, or by lithography plus dry or wet etching of non-photosensitive type. From the variety of PI surface modification techniques the discussions were focused on main efficient ones, namely rubbing with textile materials and dynamic plowing lithography (DPL). Also, a novel approach is proposed, which consists in imprinting PI surface topography with the texture of a sheared LC matrix. The processing techniques are discussed in correlation with the remaining unsolved problems in the field, attempting to bring some contributions from this point of view.

4.2.1. Influence of textile fiber characteristics on pi morphology patterned by rubbing

Modification of polyimide morphology is one of key factors in designing LCD devices with wide viewing angle and high resolution [58]. Generally, they are unidirectional rubbed with a cloth to uniformly align the LC molecules and to generate an appropriate LC pretilt angle defined as the angle between the LC director and the AL surface plane, preventing the creation of disclinations in the LC cells [59]. The PI chemical structures greatly affect the pretilt angles. Although at industrial scale rubbing is the most used technique for topography patterning, there are still some drawbacks that could be overcome so that the LC alignment mechanism would be fully elucidated. For instance, the detailed mechanism controlling the LC alignment and the pretilt angles are not yet fully understood. Many studies have been reported on this problem by taking into consideration the following aspects: rubbing parameters (force, density and strength) [59,60], annealing [61], soaking solvent [62], surface wetting characteristics [63,64]. One possibility is that alignment is induced by grooves formed mechanically on the polymer surface by the rubbing process [65]. An alternative concept is that alignment acts through the van der Waals interactions

between LC molecules and the polymer molecules, since rubbing causes the anisotropic orientation of the polymer molecules [66-68]. In this context, there are fewer studied aspects, such as the nature and the texture of the fabric fiber and the polymer surface hardness, which are factors that have to be considered in explaining the LC alignment. It is presumed that the texture and toughness of the fabric fibers and surface mechanical properties of the polymer are strongly related with the stability and dimensions of the features created on the PI surface, thus leading to a better control to LC orientation.

In order to elucidate the influence of these factors, a fundamental research has been employed on the Epiclon-based PIs containing ether linkages in the structural unit [69], since they exhibit good transparency and the lowest dielectric constants from the above discussed PIs. The **PI4** and **PI5** films were rubbed with two types of velvet: a natural one from cotton (V_C) and a artificial one made from cellulose diacetate (V_{CD}). The texture of these fabrics is different, as shown in SEM images from Figure 10. The cotton velvet is constituted from fibers of 950 μm length and 15 μm thickness, while the cellulose one has 1.5 mm length and 25 μm thickness. Figures 12 and 13 present the AFM images of the semi-alicyclic samples **PI4** and **PI5** before rubbing treatment. The rubbing process was performed

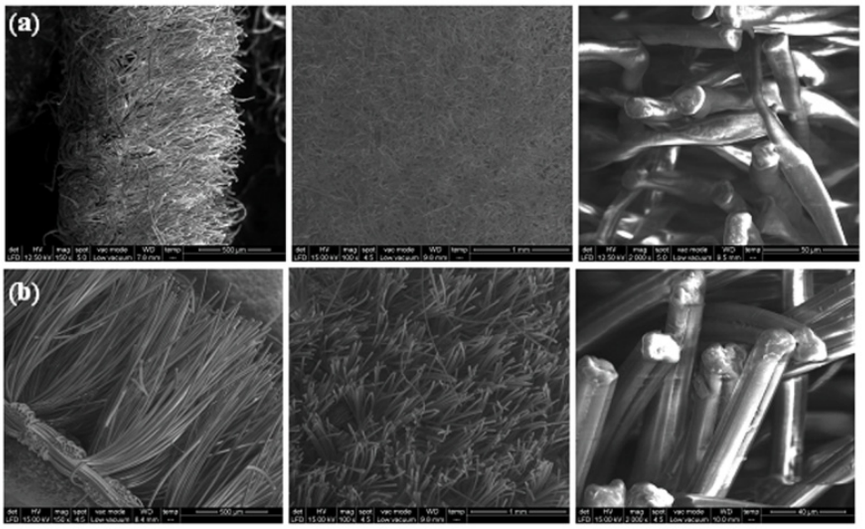

Figure 10. SEM images obtained for (a) cotton velvet and (b) velvet of cellulose diacetate

with a device, consisting in a cylinder on which was attached the velvet and the same experimental conditions were kept (100 rot/min). The surface ordering induced by rubbing is maintained over large areas (> 20x20 μm^2), but for a detailed analysis of the textile fiber effect on PI surface topography, the dimensions of the created features were examined on smaller scan areas (Figures 11 and 12). For both **PI4** and **PI5** there were obtained two dimensional and three-dimensional topographic images before and after surface ordering by rubbing. On the basis of these images, the average roughness (Sa) and percentage of surface excess (Sdr) were calculated. On each 3D image was made a diagram of the corresponding height profile of random lines, for a better visualization of the surface formations in section. Cotton velvet, although has shorter fibers compared with the artificial one, produced deeper grooves. This effect can be explained by taking into account the flexibility of the textile

fibers. Therefore, natural velvet fibers are more rigid and better penetrate the PI surface, resulting in more intense tracks. On the other hand, although artificial velvet fibers are longer, have greater flexibility leading to a greater flexion during rubbing, reducing the size of the surface grooves created on polyimides. For both samples, a better regularity of surface topography is achieved when rubbing with cotton velvet. Average roughness and surface excess percentage varied for unmodified and rubbed **PI4** and **PI5** films, according to the data presented in Table 5.

Sample	Sa (nm)	Sdr (%)	Stdi	Str	Isotropy (%)	Svi	Vmp (ml/m^2)	Vmc (ml/m^2)	Vvc (ml/m^2)	Vvv (ml/m^2)
PI4	0.3	0.12	0.79	0.35	65.80	0.07	$5.0 \cdot 10^{-5}$	$3.3 \cdot 10^{-4}$	$5.4 \cdot 10^{-4}$	$4.1 \cdot 10^{-5}$
PI4V$_C$	4.0	3.59	0.20	0.03	5.91	0.13	$2.1 \cdot 10^{-4}$	$4.5 \cdot 10^{-3}$	$5.6 \cdot 10^{-3}$	$6.7 \cdot 10^{-4}$
PI4V$_{CD}$	2.2	1.06	0.28	0.04	6.49	0.12	$1.3 \cdot 10^{-4}$	$2.4 \cdot 10^{-3}$	$3.2 \cdot 10^{-3}$	$3.5 \cdot 10^{-4}$
PI5	1.3	1.61	0.68	0.54	63.2	0.09	$1.2 \cdot 10^{-4}$	$1.5 \cdot 10^{-3}$	$2.0 \cdot 10^{-3}$	$1.6 \cdot 10^{-4}$
PI5V$_C$	4.7	3.21	0.19	0.05	5.01	0.11	$3.0 \cdot 10^{-4}$	$5.2 \cdot 10^{-3}$	$7.2 \cdot 10^{-3}$	$6.7 \cdot 10^{-4}$
PI5V$_{CD}$	3.0	1.36	0.23	0.06	9.10	0.13	$3.1 \cdot 10^{-4}$	$3.0 \cdot 10^{-3}$	$4.6 \cdot 10^{-3}$	$5.6 \cdot 10^{-4}$

Table 5. Roughness parameters calculated from AFM data for unmodified and rubbed **PI4** and **PI5**

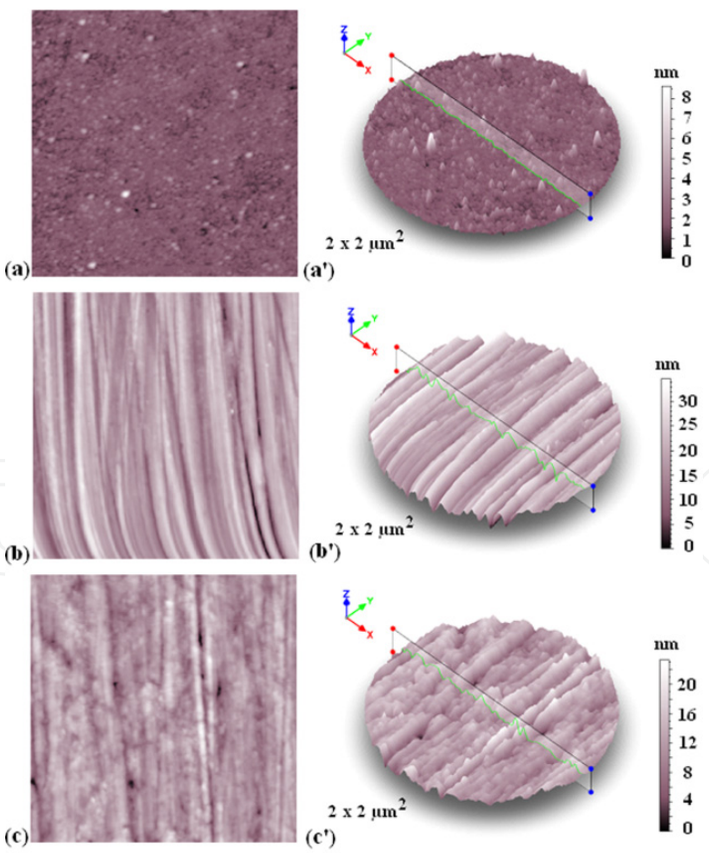

Figure 11. Bi-dimensional and three-dimensional tapping mode AFM images obtained for **PI4** polyimide film before (a, a') and after nanostructuring process induced by rubbing with a cotton velvet (b, b') and a velvet of cellulose diacetate (c, c')

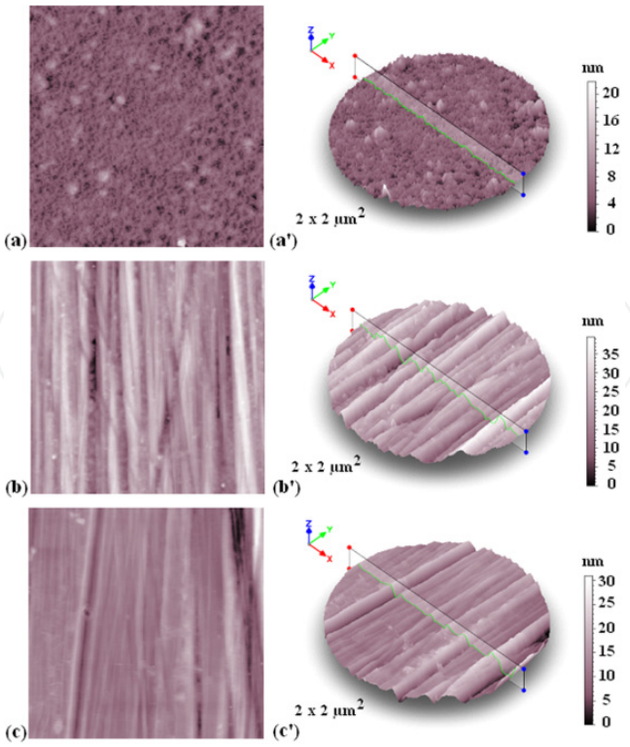

Figure 12. Bi-dimensional and three-dimensional tapping mode AFM images obtained for **PI5** polyimide film before (a, a') and after nanostructuring process induced by rubbing with a cotton velvet (b, b') and a velvet of cellulose diacetate (c, c')

Regarding this, in both PI films, the utilization of cotton velvet led to nanostructuring of the surface which changed significantly roughness parameters.

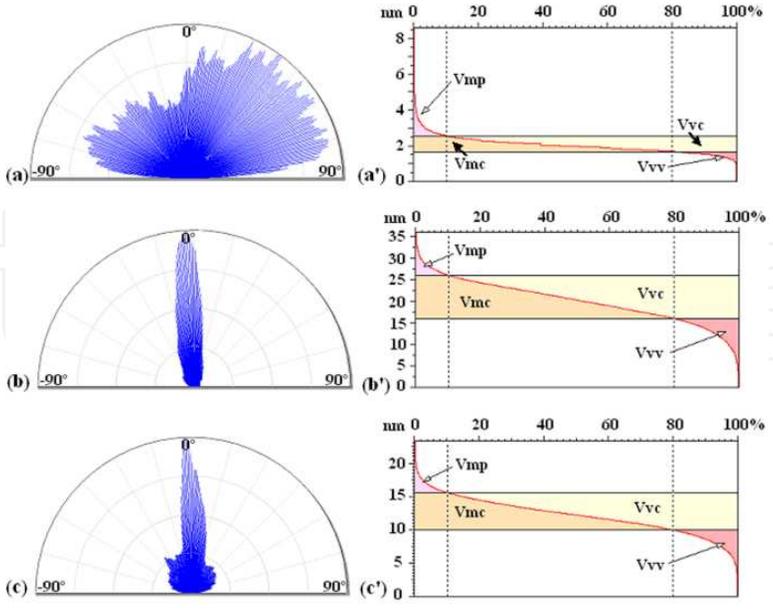

Figure 13. Angular spectra used for determination of the spatial parameters and Abbott-Firestone curves used for calculation of the volume functional parameters, obtained for **PI4** film before (a, a') and after nanostructuring process induced by rubbing with a cotton velvet (b, b') and a velvet of cellulose diacetate (c, c')

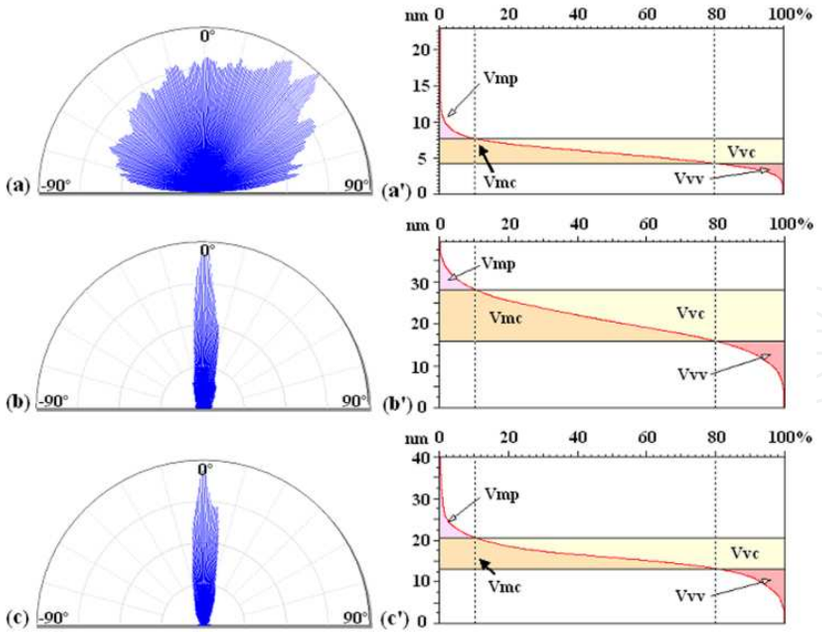

Figure 14. Angular spectra used for determination of the spatial parameters and Abbott-Firestone curves used for calculation of the volume functional parameters, obtained for **PI4** film before (a, a') and after nanostructuring process induced by rubbing with a cotton velvet (b, b') and a velvet of cellulose diacetate (c, c')

A possible mechanism of surface ordering by rubbing is that during this process local heating is produced. Thus, the mechanical stress, and thereby increasing temperature generally results in a increase in malleability of the polyimide film surface. Moreover the alignment between LC molecules and the polymer molecules acts not only through the van der Waals forces, but also through the electrostatic forces induced by rubbing.

The angular spectra from Figures 13 and 14 for **PI4** and **PI5** reveal the generation of a surface anisotropy after rubbing process. It can be observed that for unmodified samples, the formations at the film surface are not oriented by a preferred direction, but randomly. The surface isotropy of **PI4** is of 65.80%, while for **PI5** is 63.20%. Surface isotropy has decreased considerably after the rubbing process of PI films, thus the surfaces become anisotropic due to the occurrence of ordered nanostructures in the direction of rubbing. Patterning the topography with cotton velvet leads to a more regular structure, this being confirmed by lower values obtained for isotropy of 5.91% (for **PI4**) and 5.01% (for **PI5**), compared with those obtained using cellulose diacetate velvet namely: 6.49% and 9.10% respectively for **PI4** and **PI5**. These values are supported by the Stdi index, which shows the degree of surface orientation, and by Str index which accounts for the ratio aspect of the texture. Orientation indices are smaller for unmodified PIs, according to Table 5. A similar tendency is observed also for the texture indices. These parameters indicate that a more pronounced anisotropy is achieved by rubbing with cotton velvet. Volume functional parameters (Vmp, Vmc, Vvc, Vvv), calculated from Abbott-Firestone curve, as plotted in Figures 13 and 14 for Epiclon-derived PIs, were used to evidence the improvements in surface adhesion after rubbing. For both **PI4** and **PI5**, these parameters increased during surface nanostructuring with cotton velvet, comparatively with unmodified samples.

Another influencing factor on the surface ordering is represented by the PI chemical structure. Grooves produced on the **PI5** film surface are slightly smaller and denser than on the film surface **PI4**, regardless of the material used in rubbing process. For both PIs, a great difference in the depth and number of grooves created with the two types of textiles it can be noticed: the distinct topologies could be correlated with the flexibility or different mechanical properties of the two structures. During the rubbing process, a tough polymer will be less distorted, producing a weak structure, whereas a polymer with high ductility will be slightly distorted, forming a better shaped structure. Therefore, in the case of **PI5**, which is slightly more flexible than **PI4** sample, one can distinguish more surface features. It can be concluded that the pattern created on PIs based on Epiclon is finer comparatively with other PIs processed by rubbing [70]. All these mentioned aspects recommend these semi-alicyclic PIs as orientation layers for LCDs.

4.2.2. Importance of mechanical surface properties on PI morphology patterned by DPL

Another method of patterning polyimide morphology implies a modern concept based on atomic force interactions between the AFM tip and the material. Dynamic Plowing Lithography (DPL) leads to the creation of nanometric channels on film surface. The dimension of the resulted pattern depends not only on the applied force, but also on the structural organization of the polymer. As observed in Figure 15 from height profiles the nanochannels created in **PI4** film surface are of 45 nm depth and 50 nm wide, while for the **PI5** film they have smaller dimensions, namely 10 nm depth and 20 nm wide. The surface ordering induced by DPL in case of Epiclon-derived PIs is more pronounced comparatively with other commercial PIs [71], making them more suitable for LCDs applications. The differences regarding the size of the nanochannels for **PI4** and **PI5** can be correlated with their surface mechanical properties. These characteristics were evaluated from withdraw force after AFM tip penetration into the PI surface. AFM lithography was performed in contact mode using a Si cantilever, characterized by a spring constant K_e =0.03 N/m (provided by the manufacturer). Topography images were used to obtain force-distance curves over an entire image frame. Figure 16 shows two representative experimental force curves, describing the approach and retract of the AFM tip from the PI surface. Thus, after the tip is approaching the sample surface and applies a constant and default force upon the surface that leads to sample indentation and cantilever deflection, the tip tries to retract and to break loose from the surface.

Various adhesive forces between the sample and the AFM tip hamper its retraction. These adhesive forces can be calculated directly from the force-distance curves, as seen in Figure 16. Finally, the tip withdraws and looses contact to the surface upon overcoming of the adhesive forces (at level 0). Therefore, the surface hardness can be investigated through the force-distance curves, offering information on flexibility and chain packing. The withdraw force is equal with the adhesion force and can be determined from Hooke's law:

$$F = K_e \cdot \Delta x \tag{11}$$

where Δx is the cantilever shift in rapport with PI film surface.

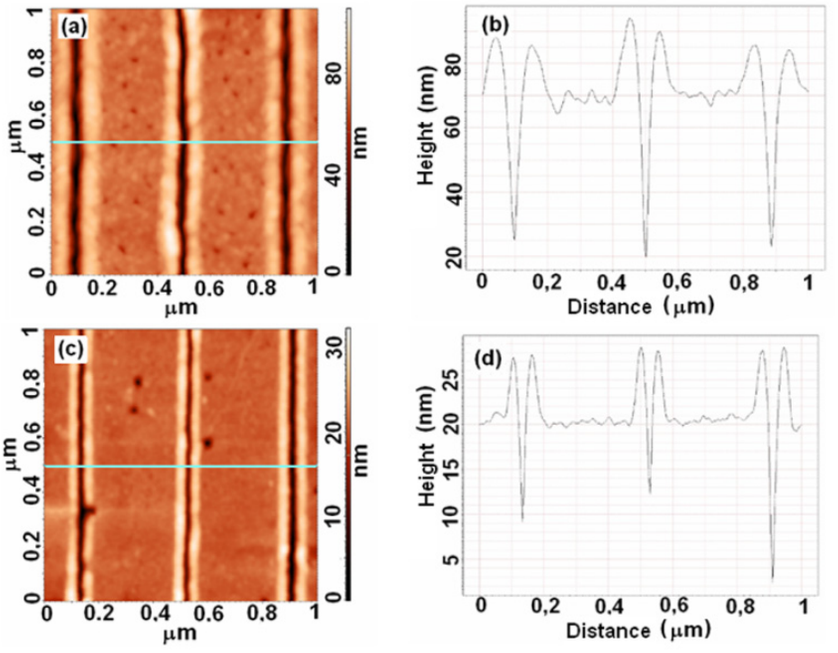

Figure 15. AFM images of (a,b) **PI4** and (c,d) **PI5** films patterned by DPL

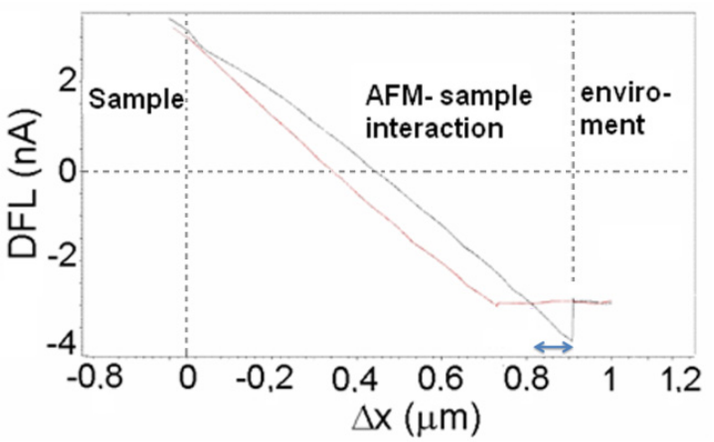

Figure 16. Typical force-distance curve showing the adhesion force for **PI4** film

The adhesion forces for **PI4** and **PI5** films, determined from expression (11), were 2.94 nN and 1.51 nN, respectively. It can be observed that adhesion force for **PI4** is slightly higher than that of **PI5**, which is in agreement with the data concerning the surface features obtained by rubbing. In this way, it can be appreciated that **PI5** exhibits, due to its higher flexibility, a better structural organization, thus explaining the smaller depths of the nanochannels produced by DPL. This type of polyimide has a patterned morphology suitable for LCDs or cell culture substrates.

4.2.3. Patterning PI surface with sheared LC matrix

A new approach for patterning polyimide, starting from its precursor, consists in using a lyotropic liquid crystal template, , namely hydroxypropyl cellulose (HPC), which under

shear conditions exhibits a banded texture [72,73] (Figure 17). Besides the specific interactions, such as the hydrogen bonds between Epiclon-based PAA corresponding to **PI4** and the LC component, a slight cross-linking produced in the precursor structure by UV irradiation can be applied to stabilize the resulting morphology. The effect of UV exposure and the influence of **HPC** weight ratio on the developed morphology are reflected in the different intensities and dimensions of the induced bands. The generated texture in the PI precursor film can be distinguished even at low lyotropic content and is also maintained after its removal with a selective solvent, namely acetone.

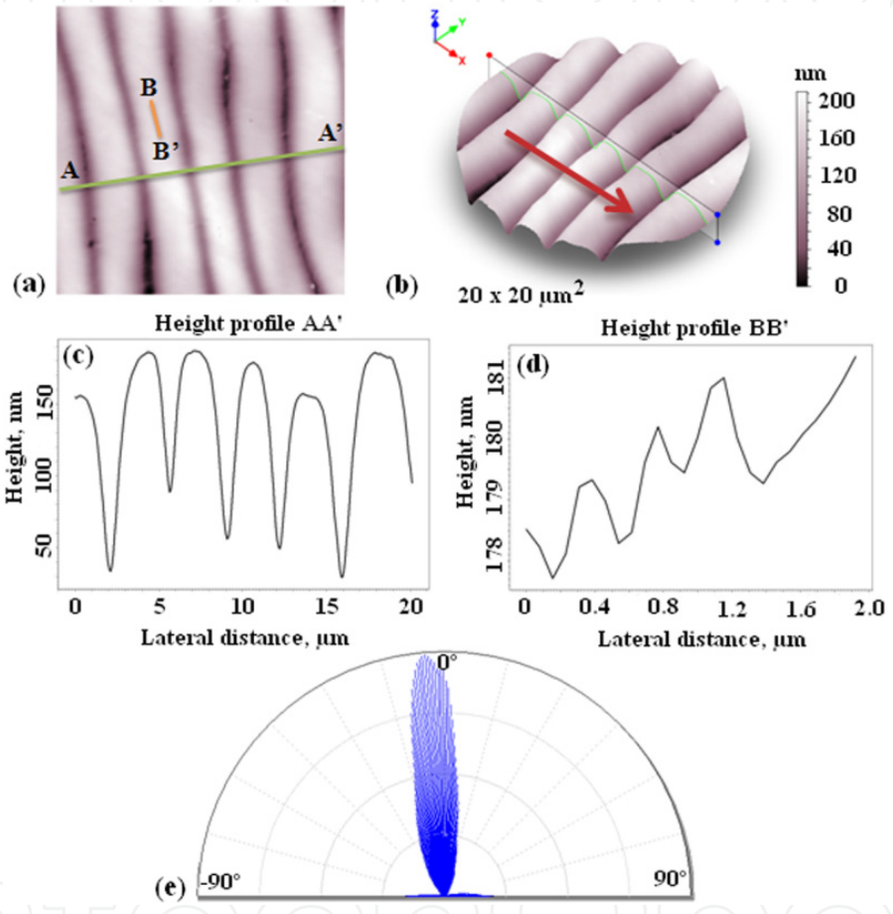

Figure 17. AFM images for **HPC** in lyotropic phase: (a) 2D-image, (b) 3D-image, (c) cross-section profiles parallel (AA') and (d) perpendicular (BB') to shear direction and (e) angular spectrum

At an equal ratio of **50 PAA/50 HPC**, the possibility of interaction between the two components increases, leading to a higher degree of ordering reflected through the formation of the third set of bands, observed only for this composition (the profile taken along the CC' direction from the 2D AFM image in Figure 18. The primary bands of the 50/50 PAA/HPC film are characterized by 6.1 μm width and 43 nm height.

The resulted surface structure can be explained using the schematic representation from Figure 19. It is well known that the free surface of a sheared HPC consists in a fibrillar morphology, with the fibrils (which are considered to be made of oriented HPC molecules) running sinusoidally along the shearing direction [74].

The primary bands are formed as a direct consequence of the sinusoidal variation in the fibrillar trajectory. When a polarizer is parallel to the shear direction, bright areas are observed where the fibril is at an angle to the shear direction, and dark areas are observed at the peaks and valleys of the sinusoidal trajectory of the fibril where the fibril is parallel to the shear direction. Thus, when large numbers of fibrils are stacked together, a banded structure is observed, with the bands running normal to the direction of shear. Bright bands are separated by dark lines which are remarked where the peaks and valleys of adjacent fibrils are registered. The secondary bands which are called "torsads" are believed to be produced as a consequence of the hydrodynamics of solvent evaporation. This situation corresponds to the structure from Figure 17. By addition of **PAA** in the system the dimensions of the large bands increase because the hydrogen bonds might lead to the stretching of the **HPC** serpentine fibers. The effect is accentuated as the content of PAA is increased – situation sustained by AFM images [72,73]. The imidization process does not affect the aspect of the final surface texture, as presented in Figure 20. The average width of the "large" bands is approximately the same before taking out **HPC**, namely 6.6 μm, while the height is larger than 120 nm. The secondary pattern is easily modified, while the third set of bands is no longer visible. The distance between the primary bands is of 4.5 μm, being a little larger after **HPC** removal. In case of directly patterning the polyimide (by this method), the band texture is larger comparatively with the poly(amic acid), and also increases with decreasing the amount of liquid crystal matrix. However, the shape of the bands is less defined probably due to the lack of hydrogen bonds. Given the surface molecular oriented Epiclon-based poly(amic acid) film, the induced alignment mechanism might be included in the category of anisotropic LC orientational elasticity in connection with an induced surface pattern. The alignment behavior of N-(4-methoxybenzylidene)-4-butylaniline (MBBA) nematic liquid crystal on patterned PI precursor was investigated (Figure 21).

Polarized Light Microscopy (PLM) revealed successively disposed dark and bright states, which change their luminosity by rotating the sample between crossed polarizers. The dark region in Figure 21a was obtained at 0° and 90° rotation of the sample director with respect to the crossed polarizers, indicating that the liquid crystal director is aligned parallel to the polarizer transmission direction. By rotating the sample from this position at 45° and 135° with respect to the crossed polarizers, bright states are observed because electric field components passing through the easy direction of MBBA give the highest resultant on the analyzer transmission direction, as revealed in Figure 21b. This behaviour is characteristic for homogeneous alignment of a liquid crystal. The high contrast between the dark and bright images indicates that the liquid crystal alignment is quite uniform.

Pure and applied research related to the shear induced morphology and structural relaxation after cessation of shear in polymer/LCP blends will become more and more important for developing high performance alignment layers used in display devices and cell culture substrates with tuned surface morphology.

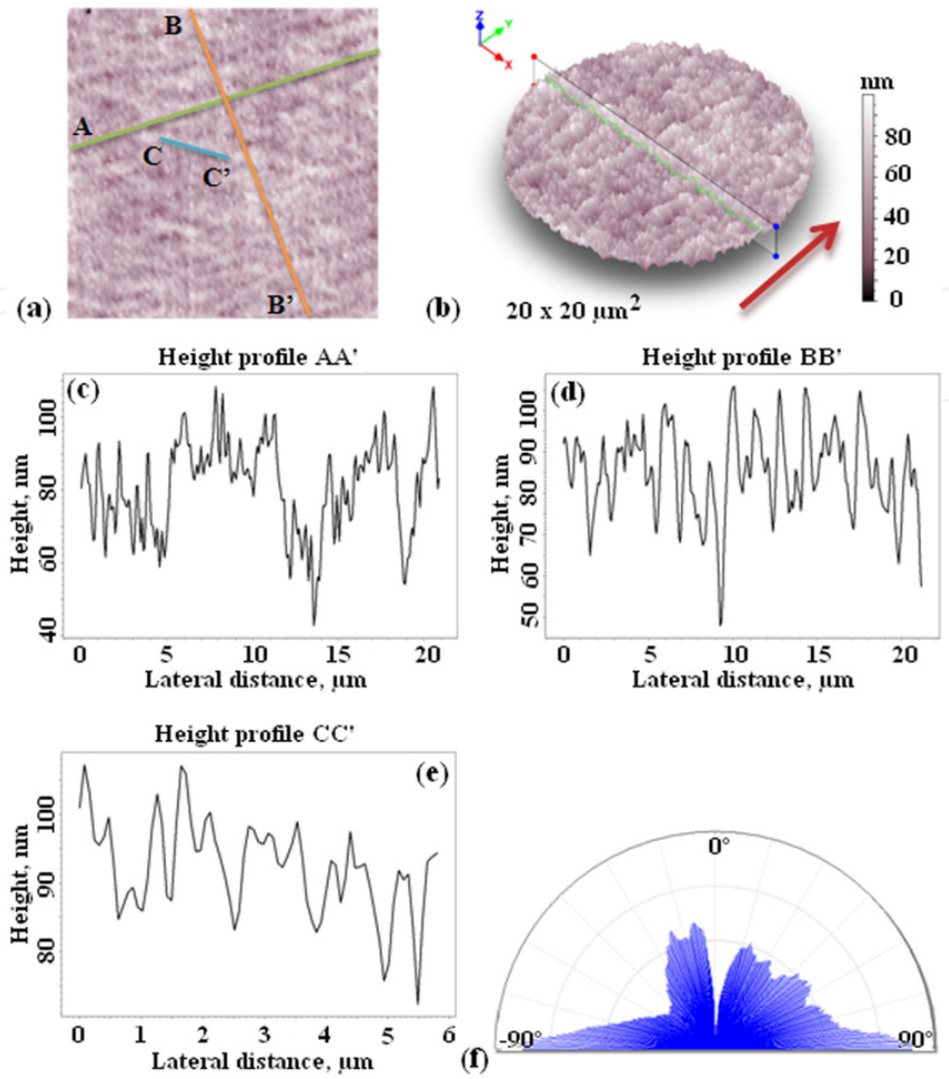

Figure 18. AFM images for **50 PAA/50 HPC**: (a) 2D-image, (b) 3D-image, (c) cross-section profiles parallel (AA') and (d) perpendicular (BB') to shear direction, (e) profile after CC' and (f) angular spectrum

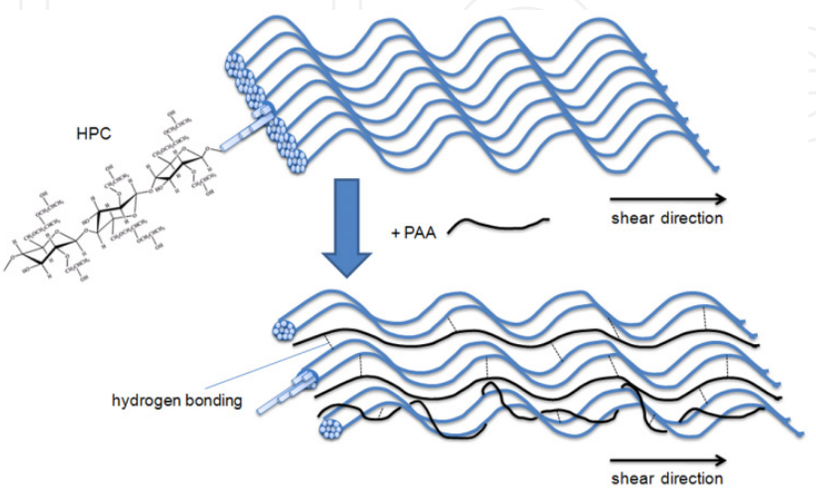

Figure 19. Schematic representation of the formation of surface banded structure in PAA/HPC

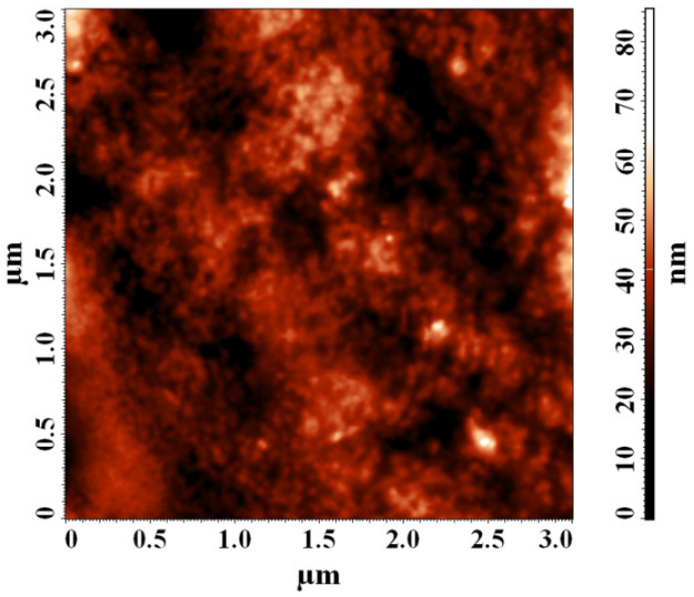

Figure 20. AFM image of imidized **PAA** after patterning with **HPC** and its removal with acetone

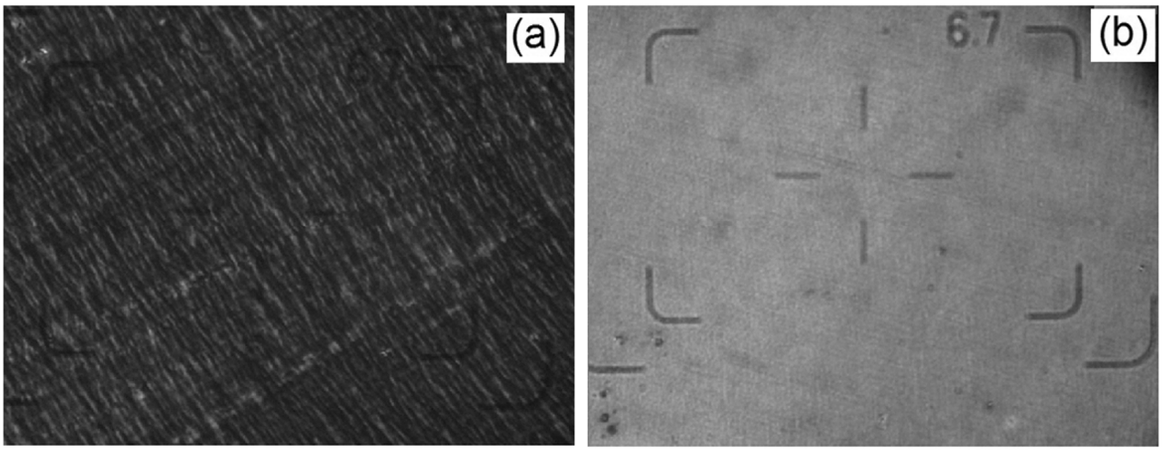

Figure 21. PLM images of MBBA on the molecular orientated **PAA** revealing (a) dark states at 0° rotation of the sample director with respect to the crossed polarizers and (b) bright states at 45° rotation of the sample director with respect to the crossed polarizers

5. Conclusion

The introduction of flexible, alicyclic Epiclon structure in the PI backbone in combination with some flexible aromatic diamines reduces the inter- and intramolecular CTC interactions, and consequently the polarizability. This approach leads to transparent materials as revealed from the refractive index values (1.6-1.7) and optical gap energies (> 3.26 eV). Also, the extinction coefficient evaluated by ellipsometry indicates that these semi-alicyclic PIs do not absorb visible light. The dielectric constant values for the samples containing ether bridges in the structural unit are lower than the classic dielectrics, namely 2.8 at 1 MHz. Moreover, their good transparency can be exploited in many applications such as LCDs or cell culture substrates. For these goals, the

morphology of PIs was patterned by rubbing, DPL and by imprinting with a sheared lyotropic LC matrix. The dimensions of the created pattern depend on nature and the texture of the fabric fiber, but also on the polymer surface mechanical properties. The greater structural organization of PI5 allows finer pattern features at the surface, both by rubbing and DPL. Orientation of PI4 precursor morphology through a LC matrix is a low cost and simple approach to obtain a banded topography, with dimensions tunable by the LC content. Also, hydrogen bonds play an important role in stabilization of the desired morphology. The dimensions of the bands are not affected after the removal of HPC with acetone and after the imidization of PAA. Future studies will be focused on the influence of diamine structure on the developed morphology with this method. Also, cell culture studies will be performed and the efficiency of employed patterning techniques will be investigated.

Author details

Andreea Irina Barzic, Iuliana Stoica and Camelia Hulubei
"Petru Poni" Institute of Macromoleculari Chemistry,
Iasi, Romania

Acknowledgement

Part of this material represents the subject of the PhD thesis of Irina Barzic, elaborated under the guidance of Dr. Silvia Ioan – Senior Researcher from "Petru Poni" Institute of Macromolecular Chemistry. This author whishes to express the most sincere and deepest gratitude to her supervisor, which by her academic achievement and contribution had remarkable influence on her student entire career, being a model as scientist, mentor, and teacher. Also, the Project PN-II-ID-PCE-2011-3-0937, No. 302/5.10.2011 is acknowledged for the financial support of this work.

6. References

[1] Ghosh MK, Mittal KL. Polyimides: fundamentals and applications. New York: Marcel Dekker Inc; 1996.
[2] Kim SI, Ree M, Shin TJ, Jung JC. Synthesis of new aromatic polyimides with various side chains containing a biphenyl mesogen unit and their abilities to control liquid-crystal alignments on the rubbed surface. J. Polym. Sci. Part A 1999;37 2909-2921.
[3] Mathews AS, Kim I, Ha C-S.Synthesis, Characterization, and Properties of Fully Aliphatic Polyimides and Their Derivatives for Microelectronics and Optoelectronics Applications. Macromol. Res. 2007;15 114-128.
[4] Richardson RR Jr, Miller JA, Reichert WM. Polyimides as biomaterials: preliminary biocompatibility testing. Biomaterials 1993;14 627-635.

[5] Rousche PJ, Pellinen DS, Pivin DP Jr, Williams JC, Vetter RJ, Kipke DR. Flexible polyimide-based intracortical electrode arrays with bioactive capability. IEEE Trans Biomed Eng 2001;48 361-371.
[6] Charest JL, Bryant LE, Garcia AJ, King W (2004) Hot embossing for micropatterned cell substrates. Biomaterials 25:4767-4775.
[7] Kreuz JA, Hsiao BS, Renner CA, Goff DL. Crystalline Homopolyimides and Copolyimides Derived from 3,3',4,4'-Biphenyltetracarboxylic Dianhydride/1,3-Bis(4-aminophenoxy)benzene/ 1,12-Dodecanediamine. 1. Materials, Preparation, and Characterization. Macromolecules 1995; 28 6926-6930.
[8] Koning C, Delmotte A, Larno P, Van Mele B. Influence of polymerization conditions on melt crystallization of partially aliphatic polyimides. Polymer 1998;39 3697-3702.
[9] Eichstadt AE, Ward TC, Bagwell MD, Farr IV, Dunson McGrath JE. Structure-property relationships for a series of amorphous partially aliphatic polyimides. J. Polym. Sci. Polym. Phys. Ed. 2002;40 1503-1512.
[10] Yang CP, Chen RS, Hunk KS. Synthesis and properties of soluble colorless poly(amide–imide)s based on N,N′-bis(3-carboxyphenyl)-4,4′-oxydiphthalimide and various aromatic diamines. Polymer 2001;42 4569-4577.
[11] Jin Q, Yamashita T, Horie K. Polyimides with alicyclic diamines. II. Hydrogen abstraction and photocrosslinking reactions of benzophenone-type polyimides. J. Polym. Sci. A 1994;32 503-511.
[12] Hsiao S-H, Chen W-T. Syntheses and Properties of Aromatic Polyimides Based on 1,1-Bis[4-(4-aminophenoxy)phenyl]-1-phenyl-2,2,2-trifluoroethane and 1,1-Bis[4-(4-aminophenoxy) phenyl]-1-phenylethane. J. Polym. Res. 2003;10 95-103
[13] Schab-Balcerzak E, Grobelny L, Sobolewska A, Miniewicz A. Cycloaliphatic–aromatic polyimides based on diamines with azobenzene unit. Eur. Polym. J. 2006;42 2859-2871.
[14] Matsumoto T, Kawabata S, Takahashi R. Alicyclic Polyimides based on bicyclo[2.2.1]heptane- 2,3,5,6-tetracarboxylic 2,3-5,6-dianhydrides. High Perform. Polym. 2006; 18 719-726.
[15] Eichstadt AE, Ward TC, Bagwell MD, Farr IV, Dunson DL, McGrath JE. Synthesis and Characterization of Amorphous Partially Aliphatic Polyimide Copolymers Based on Bisphenol- A Dianhydride. Macromolecules 2002;35 7561-7568.
[16] Kim EH, Moon IK, Kim HK, Lee MH, Han SG, Yi MH. Synthesis and characterization of novel polyimide-based NLO materials from poly(hydroxy-imide)s containing alicyclic units (II). Polymer 1999;40 6157-6167.
[17] Chung CM, Cho SY, Kim SY, Moon SY. Photosensitive polyimides having N-sulfonyloxyimide and N-carbonyloxyimide groups in the main chain. Opt. Mater. 21:421-424.
[18] Mallakpour S, Zamanlou MR (2004) Synthesis of new optically active poly(amide-imide)s containing EPICLON and L-phenylalanine in the main chain by microwave irradiation and classical heating. J. Appl. Sci. 2002;91 3281-3291.
[19] Chung EY, Choi SM, Sim HB, Kim KK, Kim DS, Kim KJ, Yi MH. Synthesis and characterization of novel photosensitive polyimide based on 5-(2,5-

dioxotetrahydrofuryl)-3- methyl-3-cyclohexene-1,2-dicarboxylic anhydride. Polym. Adv. Technol. 2005;16 19-23.

[20] Hamciuc E, Lungu, R, Hulubei C, Bruma M. New Poly(Imide-Ether-Amide)s Based on Epiclon. J. Macromol. Sci. A 2006;43 247-258.

[21] Ioan S, Cosutchi AI, Hulubei C, Macocinschi D, Ioanid G. Surface and Interfacial Properties of Poly(amic acid)s and Polyimides. Polym. Eng. Sci. 2007;47 381-389.

[22] Hulubei C, Hamciuc E, Bruma M. New imide type polymers based on epiclon. Rev. Roum. Chim. 2007;52(8–9) 891-898.

[23] Hulubei C, Hamciuc E, Bruma M. New polyimides based on Epiclon. Rev. Roum. Chim. 2007;52(11) 1063-1069.

[24] Hulubei C, Popovici D. Novel polyimides containing alicyclic units. Synthesis and characterization. Rev. Roum. Chim. 2011;56(3) 209-215.

[25] Cosutchi AI, Nica S-L, Hulubei C, Homocianu M, Ioan S. Effects of the aliphatic/aromatic structure on the miscibility, thermal, optical and rheological properties of some polyimide blends. Polym. Eng. Sci. 2012; 52(7) 1429-1439.

[26] Matsumoto T. Nonaromatic Polyimides Derived from Cycloaliphatic Monomers. Macromolecules 1999;32 4933-4939.

[27] Matsumoto T, Mikami D, Hashimoto T, Kaise M, Takahashi R, Kawabata S. Alicyclic polyimides – a colorless and thermally stable polymer for opto-electronic devices. J. Phys. Conference Series 2009;187 012005, doi:10.1088/1742-6596/187/1/012005.

[28] Ogura T, Higashihara T, Ueda M. Low-CTE photosensitive polyimide based on semialicyclic poly(amic acid) and photobase generator. J. Polym. Sci. Part A 2010;481317-1323.

[29] Cosutchi AI, Hulubei C, Stoica I, Dobromir M, Ioan S. Structural and dielectric properties of some epiclon-based polyimide films. e-Polymers 2008;068:1-15. http://www.e-polymers.org/journal/abstract_shw.cfm?Abstract_id=2388

[30] Macocinschi D, Taranu A, Hulubei C, Ioan S. Solution properties of poly(amic acid)s and polyimides. Rev. Roum. Chim. 2006;51 1001-1009.

[31] Yang CP., Hsiao SH, Wu KL. Organosoluble and light-colored fluorinated polyimides derived from 2,3-bis(4-amino-2-trifluoromethylphenoxy)naphthalene and aromatic dianhydrides. Polymer 2003;44 7067-7078.

[32] Park SJ, Cho KS, Kim SH. A study on dielectric characteristics of fluorinated polyimide thin film. J. Colloid Interf. Sci. 2004;272 384-390.

[33] Huang JC, He CB, Xiao Y, Mya KY, Dai J, Siow YP. Polyimide/POSS nanocomposites: interfacial interaction, thermal properties and mechanical properties. Polymer 2003;44 4491-4499.

[34] Khalil M, Saeed S, Ahmad Z. Properties of Binary Polyimide Blends Containing Hexafluoroisopropylidene Group. J. Macromol. Sci. A 2006;44 55-63.

[35] Hariharan RS, Bhuvana M, Sarojadevi S. Structural Characterization and Properties of Organo-soluble Polyimides, Bismaleimide and Polyaspartimides Based on 4,4′-Dichloro-3,3′- Diamino Benzophenone. High Perform. Polym. 2006;18 163-184.

[36] Cosutchi AI, Hulubei C, Ioan S. Optical and dielectric properties of some polymers with imidic structure. J. Optoelectron. Adv. Mater. 2007;9 975-980.

[37] Azzam RMA, Bashara NM. Ellipsometry and Polarized Light. Amsterdam: North-Holland Physics Publishing; 1986.
[38] van Krevelen DW. Properties of Polymers. Amsterdam: Elsevier; 1972.
[39] Groh W, Zimmermann A.What is the lowest refractive index of an organic polymer?. Macromolecules 1991;24 6660-6663.
[40] Lorenz LV. Wied. Ann. Phys. 1880;11 70-103.
[41] Lorentz HA. Wied. Ann. Phys. 1880;9 641-65.
[42] Ye YS, Chen YI, Wang YZ. Synthesis and properties of low-dielectric-constant polyimides with introduced reactive fluorine polyhedral oligomeric silsesquioxanes. J. Polym. Sci. Part A 2006;44 5391-5402.
[43] Hougham G, Tesoro G, Viehbeck A. Influence of Free Volume Change on the Relative Permittivity and Refractive Index in Fluoropolyimides. Macromolecules 1996;29 3453-3456.
[44] Cosutchi AI, Hulubei C, Buda M, Botila T, Ioan S. Effects of chemical structure on the electrical properties of some polymers with imidic structure. e-Polymers 2007;067: 1-11. http://www.e-polymers.org/journal/abstract_shw.cfm?Abstract_id=1885
[45] Yi MH, Huang H, Choi K-Y. Soluble and Colorless Polyimides from Alicyclic Diamines. J. Macromol. Sci. A 1998;35 2009-2022.
[46] Thorpe MF, Tichy L. Properties and applications of amorphous materials. London: Kluwer Academic Publishers; 2000.
[47] Tauc J, Menth A, Wood DL. Optical and Magnetic Investigations of the Localized States in Semiconducting Glasses. Phys. Rev. Lett. 1970;25 749-752.
[48] Tauc J, Menth A. States in the gap. J. Non-Cryst. Solids 1972;8-10 569-585.
[49] Jarząbek B, Weszka J, Burian A, Pocztowski G. Optical properties of amorphous thin films of the Zn-P system. Thin Solid Films 1996;279 204-208.
[50] Jarząbek B, Schab-Balcerzak E, Chamenko T, Sek D, Cisowski J, Volozhin A. Optical properties of new aliphatic–aromatic co-polyimides. J. Non-Cryst. Solids 2002;299 1057-1061.
[51] Jarząbek B, Orlik T, Cisowski J, Schab-Balcerzak E, Sezk D. Optical properties of semiladder polymer foils. Acta Phys. Pol. A 2000;98 655-659.
[52] Barzic AI, Stoica I, Hulubei C. New insights correlating transparency, absorption edges with morphological features of some semi-alicyclic polyimides. send for publication in J. Phys. Chem. B 2012
[53] Chae B, Kim SB, Lee SW, Kim SI, Choi W, Lee B. Surface Morphology, Molecular Reorientation, and Liquid Crystal Alignment Properties of Rubbed Nanofilms of a Well-Defined Brush Polyimide with a Fully Rodlike Backbone. Macromolecules 2002;35 10119-10130.
[54] Gadelmawla ES, Koura MM, Maksoud TMA, Elewa IM, Soliman HH. Roughness parameters. J. Mater. Process. Technol. 2002;123 133-145.
[55] Stout KJ, Sullivan PJ, Dong WP, Mainsah E, Luo N, Mathia T, Zahouani H. The development of methods for the characterization of roughness on three dimensions. Publication no. EUR 15178 EN of the Commission of the European Communities, Luxembourg; 1994

[56] Barbato G, Carneiro K, Cuppini D, Garnaes J, Gori G, Hughes G, Jensen CP, Jørgensen JF, Jusko O, Livi S, McQuoid H, Nielsen L, Picotto GB, Wilkening G. Scanning tunneling microscopy methods for roughness and micro hardness measurements, Synthesis report for research contract with the European Union under its programme for applied metrology, 109 pages European Commission Catalogue number: CD-NA-16145 EN-C, Brussels Luxemburg; 1995.

[57] Stoica I, Barzic AI, Hulubei C, Timpu D. Statistical analysis on morphology development of some semi-alicyclic polyimides using atomic force microscopy. send for publication in Microsc. Res. Tech. 2012

[58] Yang F, Zoriniants G, Ruan L, Sambles JR. Optical anisotropy and liquid-crystal alignment properties of rubbed polyimide layers. Liq. Cryst. 2007;34 1433-1441.

[59] Paek SY. Comparative study of rubbing parameters on polyimide alignment layers and liquid crystal alignment. J. Ind. Eng. Chem. 2001;7 316-325.

[60] Takatoh K, Hasegawa M, Koden M, Itoh N, Hasegawa R, Sakamoto M. Alignment Technologies and Applications of Liquid Crystal Devices. London and New York: Taylor and Francis; 2005.

[61] Hirosawa I, Koganezawa T, Ishii H, Sakai T. Effects of Annealing on Rubbed Polyimide Surface Studiedby Grazing-Incidence X-Ray Diffraction. IEICE Transactions on Electronics 2009; E92.C 1376-1381.

[62] Hirosawa I, Matsushita T, Miyairi H, Saito S. Effect of Soaking in Solvents on Molecular Orientation of Rubbed Polyimide Film. Jpn. J. Appl. Phys. 1999;38 2851-2855.

[63] Zheng W, Wang CC, Wang SP, Ko CL. Surface Wettability of Rubbed Polyimide Thin Films. Mol. Cryst. Liq. Cryst. 2009;512 81-90.

[64] Son PK, Choi SW. Preferred Pretilt Direction of Liquid Crystal Molecules on Rubbed Polyimide Surfaces. J. Korean Phys. Soc. 2010;57 207-209.

[65] Castellano JA. Surface Anchoring of Liquid Crystal Molecules on Various Substrates. Mol. Cryst. Liq. Cryst. 1983;94 33-41.

[66] Fukuro H, Kobayashi S. Newly Synthesized Polyimide for Aligning Nematic Liquid Crystals Accompanying High Pretilt Angles. Mol. Cryst. Liq. Cryst. 1988;163 157-162.

[67] Oo TN, Iwata T, Kimura M, Aakahane T. Surface alignment of liquid crystal multilayers evaporated on photoaligned polyimide film observed by surface profiler. Sci. Technol. Adv. Mater. 2005;6 149-157.

[68] Xiao L, Jia L, Li H, Hong T, Xu SY. Electric force microscopy study of the surface electrostatic property of rubbed polyimide alignment layers. Thin Solid Films 2000;370 238-242.

[69] Stoica I, Barzic AI, Hulubei C. The impact of rubbing fabric type on surface roughness and tribological properties of some semi-alicyclic polyimides evaluated from atomic force measurements. send for publication in Appl. Surf. Sci. 2012

[70] Chae B, Lee SW, Lee B, Choi W, Kim SB, Jung YM, Jung JC, Lee KH, Ree M. Sequence of Rubbing-Induced Molecular Segmental Reorientations in the Nanoscale Film Surface of a Brush Polymer Rod. J. Phys. Chem. B 2003;107 11911-11916.

[71] Kim JH, Yoneya M, Yamamoto J, Yokoyama H. Nano-rubbing of a liquid crystal alignment layer by an atomic force microscope: a detailed characterization. Nanotechnology 2002;13 133-137.

[72] Cosutchi AI, Hulubei C, Stoica I, Ioan S. Morphological and structural-rheological relationship in epiclon-based polyimide/hydroxypropylcellulose blend systems. J. Polym. Res. 2010;17 541-550.

[73] Cosutchi AI, Hulubei C, Stoica I, Ioan S. A new approach for patterning epiclon-based polyimide precursor films using a lyotropic liquid crystal template. J. Polym. Res. 2011;18 2389-2402.

[74] Patnaik SS, Bunning TJ, Adams WW. Atomic force microscopy and high-resolution scanning electron microscopy study of the banded surface morphology of hydroxypropyl cellulose thin films. Macromolecules 1995;28 393-395.